PAPER • OPEN ACCESS

Combining steady-state photo-capacitance spectra with first-principles calculations: the case of Fe and Ti in β-Ga_2O_3

To cite this article: C Zimmermann *et al* 2020 *New J. Phys.* **22** 063033

New Journal of Physics
The open access journal at the forefront of physics

Deutsche Physikalische Gesellschaft DPG
IOP Institute of Physics

Published in partnership with: Deutsche Physikalische Gesellschaft and the Institute of Physics

OPEN ACCESS

RECEIVED
4 March 2020

REVISED
19 April 2020

ACCEPTED FOR PUBLICATION
29 April 2020

PUBLISHED
19 June 2020

PAPER

Combining steady-state photo-capacitance spectra with first-principles calculations: the case of Fe and Ti in β-Ga_2O_3

C Zimmermann[1,3], Y Kalmann Frodason[1], V Rønning[1], J B Varley[2] and L Vines[1]

[1] Department of Physics/Centre for Materials Science and Nanotechnology, University of Oslo, P.O. Box 1048, Blindern, Oslo N-0316, Norway
[2] Lawrence Livermore National Laboratory, Livermore, CA 94550 United States of America
[3] Author to whom any correspondence should be addressed.

E-mail: christian.zimmermann@fys.uio.no

Keywords: defects in semiconductors, steady-state photo-capacitance, first-principles calculations, β-Ga_2O_3, deep-level transient spectroscopy, wide band gap semiconductors

Abstract

In this study, we demonstrate an approach to identify defects in wide band gap semiconductors by comparing accumulatively-recorded derivative steady-state photo-capacitance (SSPC) spectra to simulations using results from first-principles calculations. Specifically, we present a method to simulate SSPC spectra which adopts inputs both from first-principles calculations and the experimental conditions. The applicability of the developed method is demonstrated using the cases of subsitutional Fe (Fe_{Ga}) and Ti (Ti_{Ga}) defects in β-Ga_2O_3. Using deep-level transient spectroscopy, we identify defect levels associated with $Fe_{GaI}^{0/-}$ ($E_A = 0.66$ eV), $Fe_{GaII}^{0/-}$ ($E_A = 0.79$ eV) and $Ti_{GaII}^{+/0}$ ($E_A = 1.03$ eV) in the β-Ga_2O_3 samples studied here. Accumulatively-recorded SSPC spectra reveal several defect levels labeled T_1^{EFG}–T_6^{EFG} with onsets for optical absorption between 1.5 eV and 4.3 eV. The signature T_1^{EFG} consists of several overlapping defect signatures, and is identified as being related to $Fe_{GaI}^{0/-}$, $Fe_{GaII}^{0/-}$ and $Ti_{GaII}^{+/0}$ by comparing measured and simulated accumulatively-recorded derivative SSPC spectra.

1. Introduction

Defects have a pronounced influence on the electrical and optical properties of semiconductors, and are fundamentally important in determining the expected performance of a given semiconductor device. Often, defects are studied by using their charge state transition levels (defect levels) as fingerprints, while their unambiguous identification requires the simultaneous utilization of a number of techniques [1, 2]. In recent years, many wide band gap semiconductors, such as monoclinic gallium sesquioxide (β-Ga_2O_3), have attracted considerable research interest due to promising properties for applications ranging from photo-detectors to power electronics [3–6]. It is, however, a particular challenge to study the electronic properties of defect levels in wide band gap semiconductors.

A widely-used technique to study defect levels in semiconductors is deep-level transient spectroscopy (DLTS) [1, 7], but the accessible part of the band gap is typically limited by the temperature range used for the measurement because DLTS probes defect levels by measuring the thermally-induced emission of charge carriers from defects (traps). For example, in the case of β-Ga_2O_3, defect levels up to 1.4 eV below the conduction band edge can typically be observed using DLTS [8, 9]. Steady-state photo-capacitance (SSPC) measurements and related techniques [1, 10] measure the optically-induced emission of charge carriers from traps, and are complementary to DLTS measurements. Using suitable optical excitation, SSPC measurements can detect defect levels throughout the whole band gap of wide band gap semiconductors. Indeed, SSPC measurements and their transient counter-part deep-level optical spectroscopy have been

used to reveal several deep level defects in β-Ga_2O_3 [11–18]. SSPC measurements, as well as DLTS measurements, also provide the concentration of the traps associated with the observed defect levels. This enables a wide range of study designs suitable for identifying extrinsic as well as intrinsic defects.

First-principles calculations for defect levels in semiconductors have seen significant advancements in recent years, for example, by the introduction of hybrid-functionals, such as the Heyd–Scuseria–Ernzerhof (HSE) functionals [19] which yield an improved description of the atomic and electronic structure of semiconductors, as well as the degree of charge localization at defects [20]. These advances have bridged the gap between calculated defect levels and defect levels observed by techniques like DLTS [21, 22]. For β-Ga_2O_3, specific defect levels observed by DLTS have been identified and assigned to Fe_{GaI} (substitutional Fe on a tetrahedral Ga site), Fe_{GaII} (substitutional Fe on an octahedral Ga site) and Ti_{GaII} (substitutional Ti on an octahedral Ga site) by correlating computational and experimental results [8, 23]. Results from first-principles calculations can also be used to correlate signatures seen in SSPC measurements to specific defects present in a material. Specifically, the optical absorption associated with a defect level can be predicted [22, 24]. However, a clear and corroborated methodology to perform such comparisons is still missing. Particularly, the effect of experimental parameters on the spectral position of signatures seen in SSPC measurements should be taken into account.

Here, we report on a methodology to simulate SSPC spectra from results of first-principles calculations, enabling a comparison between first-principles calculations and SSPC measurements. Fe- and Ti-related charge state transition levels which have recently been identified by DLTS in β-Ga_2O_3 [8, 23] are used to verify the validity of our method, and thereby, we also identify the corresponding SSPC signatures related to Fe_{GaI}, Fe_{GaII} and Ti_{GaII} in β-Ga_2O_3.

2. Experimental details

Bulk β-Ga_2O_3 crystals grown by edge-defined film-fed growth (EFG) [25, 26] with a surface orientation of (−201) were obtained from *Tamura Corporation*. Samples measuring approximately (5 × 5) mm^2 were cut with a laser cutter. All samples were prepared for DLTS and SSPC measurements by depositing metal contacts using e-beam evaporation. The samples were cleaned inside an ultrasonic bath using acetone, isopropanol and de-ionized water prior to the metal depositions. Stacks of Ti and Al with a thickness of 10 nm and 120 nm, respectively, were deposited on the back side and used as Ohmic contacts, while front-side Ni contacts were used as semi-transparent Schottky contacts [27, 28]. First, Ni contacts with a thickness of 10 nm were deposited using a shadow mask with diameters of 300 μm, 600 μm and 900 μm. Subsequently, another layer of Ni with a thickness of 150 nm was deposited using a shadow mask with circular openings (diameter = 300 μm) which aligns with the first deposition such that the thick Ni pads are on top of the semi-transparent Ni pads. The thick Ni parts enable mechanical stability for wire-bonding. Additionally, Pd pads were deposited on top of the thick Ni part to further improve the wire-bonding.

Capacitance–voltage (CV) and current–voltage (IV) measurements were performed using a Keithley 6487 picoammeter/voltage source and either an HP4280 A or Boonton 7200 capacitance meter, respectively. CV measurements were performed at a probing frequency of 1 MHz. CV and IV measurements were performed to ensure device characteristics suitable for DLTS and SSPC measurements as well as to determine the donor concentration (N_D) of the β-Ga_2O_3 samples [1]. For analyzing CV measurements, a relative static dielectric constant (ϵ_s) of 10.2 was assumed for β-Ga_2O_3 [29].

DLTS measurements were performed using a setup described in detail in [23, 30]. The setup allows for DLTS measurements in the temperature range from 150 K to 680 K. DLTS spectra were constructed using a GS4 filter [31]. In order to obtain parameters describing traps, such as trap concentration (N_{tr}), activation energy (E_A) and apparent capture cross section (σ_{na}) DLTS spectra were simulated using a python-based script, where the λ-correction was employed to obtain N_{tr} [1, 32]. E_A is the sum of the classical activation energy for carrier capture (E_b) and the thermodynamic charge-state transition level [1, 21]. σ_{na} depends both on E_b and a prefactor (σ_0) which is, for example, dependent on the charge state of the trap [21, 33–37]. For the samples studied here, larger values for σ_0 can be expected for positively-charged traps as compared to neutral traps, whereas neutral traps are expected to exhibit larger values of σ_0 than negatively-charged traps [34, 37]. More information regarding the simulation of DLTS spectra and the λ-correction can be found in the appendix A.

SSPC measurements were performed with a setup described in detail in [28]. The photo-capacitance (C_{illum}) of the samples is recorded after illuminating the junction at a photon energy E for a time t_{illum}, whereby t_{illum} between 30 s and 1200 s were employed for this study. C_{illum} is referenced to the capacitance

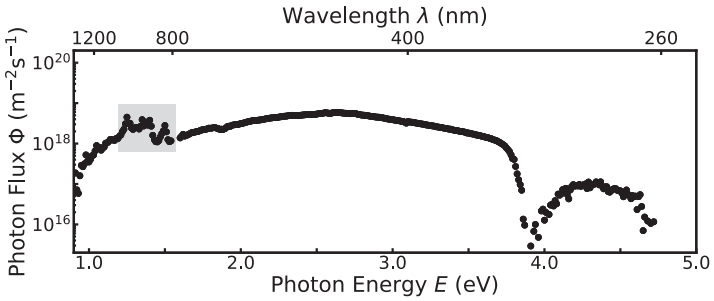

Figure 1. Photon flux $\Phi(E)$ recorded for the optical excitation used for SSPC measurements. A structure is marked in gray which also appears in SSPC measurements.

of the junction in the dark (C_{dark}). All capacitance values were measured at a fixed external bias (V_{ext}) of −8 V. SSPC spectra $S(E, t_{\mathrm{illum}})$ were recorded by subsequently measuring $C_{\mathrm{illum}}(E, t_{\mathrm{illum}})$ at different E after t_{illum}. Measurements were performed using steps (ΔE) of 20 meV in-between subsequent E. The spectral distribution of the optical excitation represented by the photon flux ($\Phi(E)$) was determined using a calibrated thermal power meter placed at the sample position, and is shown in figure 1. Typical photon fluxes of 1×10^{17} m^{-2} s^{-1} in the UV and 1×10^{19} m^{-2} s^{-1} in the visible part of the spectrum were found. SSPC spectra were recorded at 120 K.

SSPC measurements can be performed accumulatively [28] or non-accumulatively [1, 13]. For the accumulative SSPC measurements conducted here, $S(E, t_{\mathrm{illum}})$ was recorded at subsequent E without changing V_{ext}, and the measurements were exclusively performed in ascending order of E. In contrast, in non-accumulative SSPC measurements, V_{ext} is set to 0 V in-between measurements at subsequent E.

3. Methodology

3.1. First-principles calculations based on hybrid-functionals

A detailed description of the first-principles methodology and computational details can be found in [23], thus only a brief summary is given here. All calculations were performed using the Heyd–Scuseria–Ernzerhof [19] range-separated hybrid functional, as implemented in the VASP code [38], with the fraction of screened Hartree–Fock exchange set to $\alpha = 0.33$. Defect calculations were performed with 160-atom supercells, a plane-wave energy cutoff of 500 eV and a single k-point at (1/4, 1/4, 1/4). To remedy the spurious supercell-size dependence of thermodynamic and vertical charge state transition energies, we used the correction schemes of Freysoldt *et al* [39, 40], and Gake *et al* [41], respectively.

The optical properties of $\mathrm{Fe_{GaI}}$, $\mathrm{Fe_{GaII}}$ and $\mathrm{Ti_{GaII}}$ were investigated within the framework of the one-dimensional configuration coordinate (CC) model [20, 22, 42, 43]. CC diagrams were constructed using model parameters from the hybrid-functional calculations, namely the change in configuration coordinate ΔQ, the zero-phonon line (ZPL) energy E_{ZPL}, and the effective vibrational frequencies Ω_{g} and Ω_{e} in the ground (g) and excited (e) state, respectively. In the Franck–Condon (FC) approximation, optical transitions are vertical with no change in configuration coordinate. Classical emission and absorption energies can then be defined as $E_{\mathrm{em}} = E_{\mathrm{ZPL}} - d_{\mathrm{g}}^{\mathrm{FC}}$ and $E_{\mathrm{abs}} = E_{\mathrm{ZPL}} + d_{\mathrm{e}}^{\mathrm{FC}}$, respectively, where $d_{\mathrm{g}}^{\mathrm{FC}}$ and $d_{\mathrm{e}}^{\mathrm{FC}}$ are the so-called FC shifts. The normalized absorption cross-section $\sigma_{i,\mathrm{norm}}^{\mathrm{o}}(E)$, including temperature -dependent vibrational broadening, can be simulated using the effective vibrational frequencies, as outlined in [22, 24].

$\sigma_{\mathrm{n,norm}}^{\mathrm{o}}(E)$ is related to the optically-induced emission of electrons from a defect, while $\sigma_{\mathrm{p,norm}}^{\mathrm{o}}(E)$ is related to the optically-induced emission of holes. Thus, $\sigma_{\mathrm{n,norm}}^{\mathrm{o}}(E)$ is related to processes involving electrons and the conduction band edge, and $\sigma_{\mathrm{p,norm}}^{\mathrm{o}}(E)$ is associated with processes involving electrons and the valence band edge.

3.2. Simulation of steady-state photo-capacitance spectra

The SSPC signal $S(E, t_{\mathrm{illum}})$ is usually presented as [1, 10]:

$$S(E, t_{\mathrm{illum}}) = 2\frac{C_{\mathrm{illum}}(E, t_{\mathrm{illum}}) - C_{\mathrm{dark}}}{C_{\mathrm{dark}}} N_{\mathrm{D}} = 2\frac{\Delta C_{\mathrm{illum}}(E, t_{\mathrm{illum}})}{C_{\mathrm{dark}}} N_{\mathrm{D}} = N_{\mathrm{tr,eff}}^{*}(E, t_{\mathrm{illum}}). \quad (1)$$

Here, $\Delta C_{\mathrm{illum}}(E, t_{\mathrm{illum}})$ denotes the change in (photo-)capacitance during illumination for t_{illum} at E, and C_{dark} represents the capacitance of the junction measured in the dark. $N_{\mathrm{tr,eff}}^{*}(E, t_{\mathrm{illum}})$ is the change in the

concentration of ionized traps inside the probing volume due to illumination. However the probing volume will usually not be equal to the volume of the space-charge region [1, 28]. Moreover, equation (1) assumes $N_{\mathrm{D}} \ll N^{*}_{\mathrm{tr,eff}}$ to be valid.

$S\left(E, t_{\mathrm{illum}}\right)$ can be expressed with the following empirically-motivated formula [28]:

$$S\left(E, t_{\mathrm{illum}}\right) = 2N_{\mathrm{D}} \sum_{i} \frac{\Delta C_{\mathrm{illum},i}}{C_{\mathrm{dark}}} \frac{1}{1+\exp\left(-\frac{E-E_i}{\gamma_i}\right)} \tag{2}$$

where E_i denotes the onset of optical absorption related to trap i, and γ_i describes the steepness of the corresponding step in $S\left(E, t_{\mathrm{illum}}\right)$. $\Delta C_{\mathrm{illum},i}$ is the (photo-)capacitance change related to photo-excitation of trap i. $\Delta C_{\mathrm{illum},i}$ are larger than zero for optically-induced electron emission, and are smaller than zero for optically-induced hole emission. Results of SSPC measurements can also be presented as derivative SSPC spectra $\mathrm{d}S\left(E, t_{\mathrm{illum}}\right)/\mathrm{d}E$ [10, 28, 44]. Peaks at E_i in $\mathrm{d}S\left(E, t_{\mathrm{illum}}\right)/\mathrm{d}E$ will represent trap i [28]. Notably, the optically-induced emission of a charge carrier only contributes to the recorded $S\left(E, t_{\mathrm{illum}}\right)$ if the charge carrier is swept out of the space-charge region by the electrical field present in the space-charge region. For many semiconducting oxides, self-trapped holes or electrons can form which may not be sufficiently mobile to leave the space-charge region [45]. In β-Ga_2O_3, self-trapped holes are expected to form with very low mobility below room temperature [45, 46].

In steady-state, i.e., for sufficiently long t_{illum}, $S\left(E, t_{\mathrm{illum}}\right)$ will be constant, and equal to $N^{\mathrm{ss}}_{\mathrm{tr,eff}}$, representing the steady-state concentration of ionized traps inside the probing volume. $N^{\mathrm{ss}}_{\mathrm{tr,eff}}$ is a sum of all $N^{\mathrm{ss}}_{\mathrm{tr,eff},i}$ representing the concentration of ionized traps i in steady-state. If optically-induced hole emission can be neglected, $N_{\mathrm{tr},i}$ can be computed from $N^{\mathrm{ss}}_{\mathrm{tr,eff},i}$ via [1]:

$$N_{\mathrm{tr},i} = N^{\mathrm{ss}}_{\mathrm{tr,eff},i} \frac{W^2}{x_{1,i}^2 - W_{\mathrm{o},i}^2} = cN^{\mathrm{ss}}_{\mathrm{tr,eff},i}. \tag{3}$$

$N_{\mathrm{tr},i}$ is the actual concentration of trap i. W is the depth of the depletion layer at V_{ext}, $x_{1,i}$ is the depth where the thermodynamic charge state transition level of trap i (E_i^{th}) crosses the Fermi-level E_{F}, and $W_{\mathrm{o},i}$ represent the fact that electrons from outside the space-charge region can penetrate into the space-charge region and refill photo-ionized traps. The correction factor c represents that during SSPC measurements traps are only photo-ionized in part of the volume of the space-charge region, and will always be larger than 1. Notably, $W_{\mathrm{o},i}$ will be smaller for a trap for which electron capture is more likely [1]. Here, $W_{\mathrm{o},i}$ can be expected to be reduced for donor defects as compared to acceptor defects [34, 37]. Smaller values for $W_{\mathrm{o},i}$ suggest that traps are photo-ionized in a smaller volume inside the space-charge region, and hence the correction factor c will be larger. If hole emission cannot be neglected, an additional factor representing the relative magnitude of optically-induced electron emission as compared to optically-induced hole emission needs to be added to the right hand side of equation (3) [10]. For non-ideal junctions, further corrections in addition to equation (3) are necessary due to leakage currents inside the space-charge region [47]. If leakage currents are present, corrections based on equation (3) will underestimate the actual trap concentration. Generally, traps with larger capture cross-sections for electrons will capture more electrons from the leakage current, and hence a larger deviation from equation (3) can be expected [47].

In order to obtain computational results which can be compared to measured $S\left(E, t_{\mathrm{illum}}\right)$, one needs to compute $N^{*}_{\mathrm{tr,eff}}$ (see equation (1)). The time-evolution of $N^{*}_{\mathrm{tr,eff}}$ is described by the following differential equation [1, 10]:

$$\frac{\mathrm{d}N^{*}_{\mathrm{tr,eff}}}{\mathrm{d}t} = \sigma_{\mathrm{n}}^{\mathrm{o}} \Phi N_{\mathrm{tr,eff}} - \sigma_{\mathrm{p}}^{\mathrm{o}} \Phi N^{*}_{\mathrm{tr,eff}}. \tag{4}$$

Here, $N_{\mathrm{tr,eff}}$ denotes the concentration of traps occupied with electrons. σ_i^{o} are the absorption cross-sections related to the optically-induced emission of electrons ($i = \mathrm{n}$) or holes ($i = \mathrm{p}$) from a trap [22]. Often, optically-induced hole emission can be neglected, and one obtains:

$$\frac{\mathrm{d}N^{*}_{\mathrm{tr,eff}}}{\mathrm{d}t} = \sigma_{\mathrm{n}}^{\mathrm{o}} \Phi N_{\mathrm{tr,eff}}. \tag{5}$$

Here, $N_{\mathrm{tr,eff}}$ is equal to $N^{\mathrm{ss}}_{\mathrm{tr,eff}} - N^{*}_{\mathrm{tr,eff}}$. Equation (5) can be solved for the experimental conditions encountered in accumulative or non-accumulative SSPC measurements. In the following, E^k denotes a specific photon energy used for illumination during an SSPC measurements. The E^k are ordered in ascending order, and hence $E^k > E^{k-1}$ is valid. For accumulative SSPC measurements, one obtains the following expression for equation (1) when solving equation (5):

$$S_{\mathrm{acc}}\left(E^k, t_{\mathrm{illum}}\right) = S\left(E^{k-1}, t_{\mathrm{illum}}\right) + \left[N^{\mathrm{ss}}_{\mathrm{tr,eff}} - S\left(E^{k-1}, t_{\mathrm{illum}}\right)\right]\left[1 - \exp\left(-\sigma_{\mathrm{n}}^{\mathrm{o}}\left(E^k\right)\Phi\left(E^k\right) t_{\mathrm{illum}}\right)\right], \tag{6}$$

Table 1. Summary of parameters describing the CC diagrams for $Fe_{GaI}^{0/-}$, $Fe_{GaII}^{0/-}$ and $Ti_{GaII}^{+/0}$ [8, 23].

Defect	E_{ZPL} (eV)	$d_{g/e}^{FC}$ (eV)	ΔQ (amu$^{1/2}$/Å)	$\Omega_{g/e}$ (meV)
$Fe_{GaI}^{0/-}$	0.62	1.10/1.02	1.63	59/57
$Fe_{GaII}^{0/-}$	0.72	1.04/0.93	1.22	76/72
$Ti_{GaII}^{+/0}$	1.13	1.01/1.14	1.35	68/72

if one specific trap is assumed to be present in the space-charge region. Notably, k starts at 1, and $S\left(E^0, t_{illum}\right)$ is set to zero.

For non-accumulative SSPC measurements, the corresponding expression is:

$$S_{non-acc}\left(E^k, t_{illum}\right) = N_{tr,eff}^{ss}\left[1 - \exp\left(-\sigma_n^o\left(E^k\right)\Phi\left(E^k\right)t_{illum}\right)\right], \tag{7}$$

if one specific trap is assumed to be present in the space-charge region. To solve equations (6) and (7), one needs to know $\sigma_n^o\left(E^k\right)$ and $\Phi\left(E^k\right)$. $\sigma_n^o\left(E^k\right)$ can be defined as:

$$\sigma_n^o\left(E^k\right) = \Sigma_n^o \sigma_{n,norm}^o\left(E^k\right). \tag{8}$$

$\sigma_{n,norm}^o$ can be obtained from first-principles calculations for a specific defect. The absolute value Σ_n^o, however, is challenging to extract from first-principles calculations, and is considered a free parameter of the simulation. $\Phi\left(E^k\right)$ was measured for the optical excitation of the setup used for SSPC measurements (see figure 1). If several traps i are present, $S_{acc}\left(E^k, t_{illum}\right)$ and $S_{non-acc}\left(E^k, t_{illum}\right)$ are superpositions of contributions $S_{acc,i}\left(E^k, t_{illum}\right)$ and $S_{non-acc,i}\left(E^k, t_{illum}\right)$ from the individual traps i, assuming no interaction between traps, which is a viable assumption in the dilute regime.

The main difference between accumulative and non-accumulative SSPC measurements is the starting point for SSPC measurements performed at subsequent E^k. Accumulative SSPC measurements will exhibit a steeper rise of $S_{acc}\left(E^k, t_{illum}\right)$ in the vicinity of defect-related optical absorption. Thus, accumulative SSPC measurements are more suitable for reaching steady-state conditions for a given trap. In the appendix A, a detailed derivation of equations (6) and (7) as well as comparisons between the theoretical expressions of $S_{acc}\left(E^k, t_{illum}\right)$ (see equation (6)) and $S_{non-acc}\left(E^k, t_{illum}\right)$ (see equation (7)) are shown.

4. Results and discussion

The CC diagrams for the charge state transitions $Fe_{GaI}^{0/-}$, $Fe_{GaII}^{0/-}$ and $Ti_{GaII}^{+/0}$ were calculated using hybrid-functionals, and the parameters describing $Fe_{GaI}^{0/-}$, $Fe_{GaII}^{0/-}$ and $Ti_{GaII}^{+/0}$ are summarized in table 1 [8, 23]. The computed values are in accordance with other recent studies regarding $Fe_{GaI}^{0/-}$ and $Fe_{GaII}^{0/-}$ [48] as well as $Ti_{GaII}^{+/0}$ [49]. Figure 2 displays results for $\sigma_{n,norm}^o$ and $\sigma_{p,norm}^o$ related to $Fe_{GaI}^{0/-}$, $Fe_{GaII}^{0/-}$ and $Ti_{GaII}^{+/0}$ in β-Ga_2O_3. A temperature of 120 K was assumed for the computations. For $\sigma_{n,norm}^o$, calculated absorption cross-section spectra are shown with and without taking vibrational broadening into account, whereas only results including vibrational broadening are shown for $\sigma_{p,norm}^o$. Calculated absorption cross-section spectra without vibrational broadening exhibit sharp onsets of absorption, and particularly, exhibit no absorption below the classical absorption energy E_{abs} [22], in contrast to what is expected in experiments. Hence, absorption cross-sections with vibrational broadening are used in the following. The calculated $\sigma_{n,norm}^o$ and $\sigma_{p,norm}^o$ are broad which is in accordance with previous computational results for $\sigma_{n,norm}^o$ related to primary intrinsic defects in β-Ga_2O_3 [28]. Note that the $\sigma_{n,norm}^o$ related to $Fe_{GaI}^{0/-}$ and $Fe_{GaII}^{0/-}$ show a significant overlap, while $\sigma_{n,norm}^o$ related to $Ti_{GaII}^{+/0}$ occurs at higher photon energies. Our computational results for $\sigma_{n,norm}^o$ of $Fe_{GaII}^{0/-}$ and $Fe_{GaI}^{0/-}$ are in accordance with experimental photo-electron paramagnetic resonance studies performed by Bhandari *et al* [48, 50]. For $Fe_{GaI}^{0/-}$, $Fe_{GaII}^{0/-}$ and $Ti_{GaII}^{+/0}$, optically-induced hole emission is only seen for photon energies close to E_g, i.e., optically-induced hole emission does not occur in the photon energy range where the onset of optically-induced electron emission is observed for these charge-state transitions. Thus, optically-induced hole emission related to $Fe_{GaI}^{0/-}$, $Fe_{GaII}^{0/-}$ and $Ti_{GaII}^{+/0}$ can be neglected when modeling SSPC spectra for photon energies lower than 4.0 eV.

Figure 3 shows DLTS spectra recorded on a EFG-grown β-Ga_2O_3 crystal. Three defect signatures labeled as E_{2a} ($E_A = 0.66$ eV, $\sigma_{na} = 4 \times 10^{-16}$ cm^2), E_{2b} ($E_A = 0.79$ eV, $\sigma_{na} = 3 \times 10^{-15}$ cm^2) and E_3 ($E_A = 1.03$ eV, $\sigma_{na} = 1 \times 10^{-13}$ cm^2) are found to be present, in accordance with previous studies on EFG-grown β-Ga_2O_3 crystals [8, 23]. No other defect levels with smaller activation energies than 1.2 eV were present in

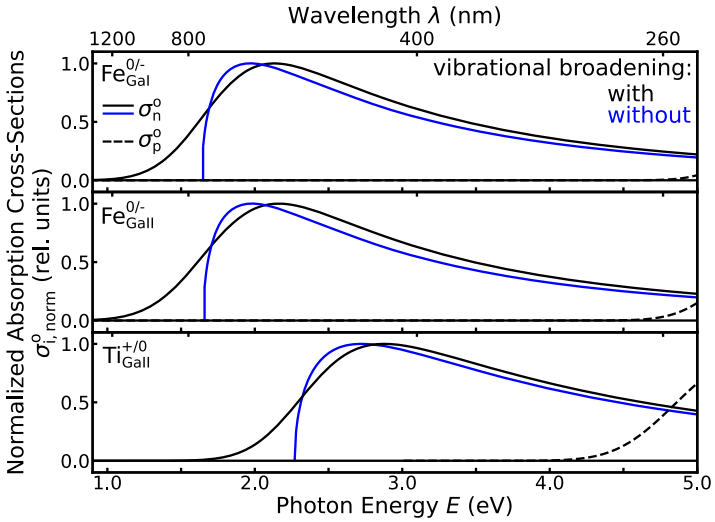

Figure 2. Absorption cross-sections $\sigma^{o}_{n,norm}$ and $\sigma^{o}_{p,norm}$ related to $Fe^{0/-}_{GaI}$, $Fe^{0/-}_{GaII}$ and $Ti^{+/0}_{GaII}$. For $\sigma^{o}_{n,norm}$, results are shown with and without taking vibrational broadening into account, while for $\sigma^{o}_{p,norm}$ results are only shown with vibrational broadening. A temperature of 120 K was assumed.

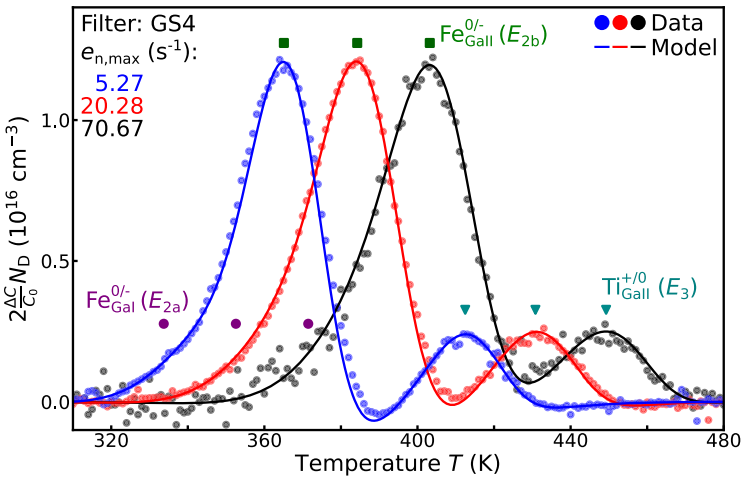

Figure 3. DLTS spectra recorded on a EFG-grown β-Ga_2O_3 crystal. The DLTS spectra were constructed with a GS4 filter and compared to simulations (solid lines). Three defect signatures $Fe^{0/-}_{GaI}$ (E_{2a}), $Fe^{0/-}_{GaII}$ (E_{2b}) and $Ti^{+/0}_{GaII}$ (E_3) are observed and labeled.

concentrations exceeding 1×10^{15} cm^{-3} in this sample. E_{2a} and E_{2b} have been assigned to $Fe^{0/-}_{GaI}$ and $Fe^{0/-}_{GaII}$, respectively [8, 23, 51], while E_3 is proposed to be related to $Ti^{+/0}_{GaII}$ [23]. This identification is consistent with a recent DLTS study that associated E_{2a}/E_{2b} with a deep acceptor and E_3 with a deep donor [52]. Taking the λ-correction [1, 32] into account, the concentrations of the corresponding traps were determined to be 2.54×10^{15} cm^{-3} (E_{2a} or Fe_{GaI}), 2.32×10^{16} cm^{-3} (E_{2b} or Fe_{GaII}) and 5.45×10^{15} cm^{-3} (E_3 or Ti_{GaII}), respectively (see table 2). Thus, using DLTS measurements, we are able to establish the presence and concentration of Fe_{GaI}, Fe_{GaII} and Ti_{GaII} in the sample.

Accumulative SSPC measurements were performed on the same EFG-grown β-Ga_2O_3 sample for which DLTS spectra are shown in figure 3. Figure 4(a) displays the recorded SSPC spectrum represented as conventional SSPC spectrum ($S_{acc}(E)$) and as derivative SSPC spectrum ($dS_{acc}(E)/dE$). Optically-induced emission of electrons is observed with onsets at 2.2–2.3 eV (T_1^{EFG}), 2.8–2.9 eV (T_2^{EFG}), 3.7–3.8 eV (T_3^{EFG}), 3.8–4.0 eV (T_4^{EFG}), 4.0–4.2 eV (T_5^{EFG}) and 4.2–4.3 eV (T_6^{EFG}). Furthermore, a signature originating from the band gap (E_g) of β-Ga_2O_3 can be seen. The features T_1^{EFG} and T_2^{EFG} are broad and partially overlap, and hence it is difficult to establish the respective onset position accurately. Interestingly, T_1^{EFG} and T_2^{EFG} can be properly distinguished in $dS_{acc}(E)/dE$ (see upper panel in figure 4(a)) which demonstrates the applicability of derivative SSPC spectra [28].

Table 2. Summary of the paramters used for the model displayed in figure 5. The values for $N^{ss}_{tr,eff}$ were determined from modeling accumulative SSPC spectra (see figure 5), while the values for N_{tr} were obtained from DLTS measurements (see figure 3).

Defect level	Σ^{o}_{n} (10^{-18} cm^2)	$N^{ss}_{tr,eff}$ (10^{15} cm^{-3})	N_{tr} (10^{15} cm^{-3})
$Fe^{0/-}_{GaI}$	0.3	1.5	2.6
$Fe^{0/-}_{GaII}$	0.3	9.5	23.2
$Ti^{+/0}_{GaII}$	9.6	1.1	5.5

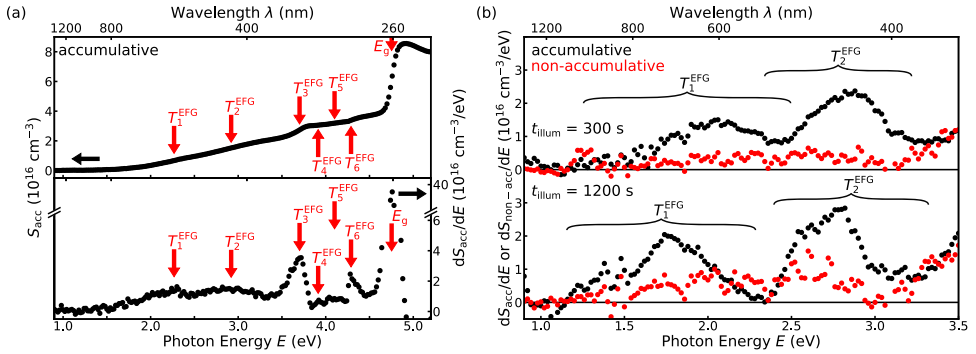

Figure 4. (a) SSPC spectrum recorded accumulatively on an EFG-grown β-Ga_2O_3 crystal ($t_{illum} = 300$ s). The results are displayed as conventional SSPC spectrum (upper panel) and derivative SSPC spectrum (lower panel). Several defect-related signatures are present and their onset positions are marked with arrows. E_g marks a signature related to the band gap of β-Ga_2O_3. (b) Comparison between derivative SSPC spectra recorded on an EFG-grown β-Ga_2O_3 crystal accumulatively and non-accumulatively using two different t_{illum}. Only the photon energy range where T^{EFG}_1 and T^{EFG}_2 occur is shown.

Figure 4(b) displays a comparison between derivative SSPC spectra recorded accumulatively as well as non-accumulatively on the same EFG-grown β-Ga_2O_3 crystal. The spectra were recorded using two different t_{illum}. Data are only shown for the photon energy range where T^{EFG}_1 and T^{EFG}_2 can be seen. Features in $dS_{acc}(E)/dE$ are narrower than the corresponding features seen in $dS_{non-acc}(E)/dE$. Indeed, it is not possible to distinguish T^{EFG}_1 and T^{EFG}_2 in $dS_{non-acc}(E)/dE$. With increasing t_{illum}, the signatures associated with T^{EFG}_1 and T^{EFG}_2 become significantly more narrow and shift to lower photon energies in $dS_{acc}(E)/dE$, while only minor changes are seen in $dS_{non-acc}(E)/dE$. Thus, using accumulative SSPC measurements with long t_{illum}, the spectral resolution can be significantly improved. The spectral shape seen for T^{EFG}_1 and T^{EFG}_2 in $dS_{acc}(E)/dE$ recorded with $t_{illum} = 1200$ s clearly suggests the presence of several overlapping defect signatures.

As mentioned before, DLTS measurements confirm the presence of $Fe^{0/-}_{GaI}$, $Fe^{0/-}_{GaII}$ and $Ti^{+/0}_{GaII}$ in this EFG-grown β-Ga_2O_3 sample, and are thus expected to appear in SSPC spectra as well. It is possible to estimate the onset of defect-related optical absorption by adding the Franck–Condon shift for a specific charge-state transition of a defect to the corresponding activation energy determined by DLTS [21, 22]. Assuming typical Franck–Condon shifts of 0.4–1.2 eV as reported in β-Ga_2O_3 previously [11, 12, 28], one expects the optical absorption related to $Fe^{0/-}_{GaI}$, $Fe^{0/-}_{GaII}$ and $Ti^{+/0}_{GaII}$ to occur at around 1.1–2.2 eV. Thus, $Fe^{0/-}_{GaI}$, $Fe^{0/-}_{GaII}$ and $Ti^{+/0}_{GaII}$ are all plausible candidates for T^{EFG}_1. Further, the amplitude of T^{EFG}_1 suggests an associated trap concentration in the range of 1×10^{16} cm^{-3}, corroborating the relation to Fe_{GaI}, Fe_{GaII} and Ti_{GaII}. Notably, we observed no other defect signatures in DLTS measurements with concentrations above 1×10^{15} cm^{-3} that are likely candidates for contributing to T^{EFG}_1.

In order to assign T^{EFG}_1 to $Fe^{0/-}_{GaI}$, $Fe^{0/-}_{GaII}$ and $Ti^{+/0}_{GaII}$, however, it is necessary to compare the calculated results for $\sigma^{o}_{n,norm}$ (see figure 2) to the recorded SSPC spectra. Particularly, it is necessary to take experimental parameters such as t_{illum} into account (see figure 4(b)). One approach is the method presented above, by comparing the experimental data with SSPC spectra simulated by utilizing the absorption cross sections obtained from first-principles calculations. In figure 5, SSPC spectra recorded accumulatively on the same EFG-grown β-Ga_2O_3 crystal for which results are shown in figure 3 are compared to simulations based on equation (6). Importantly, the overall trap concentration is found to be lower than 20% of N_D. The simulations were performed assuming only the presence of $Fe^{0/-}_{GaI}$, $Fe^{0/-}_{GaII}$ and $Ti^{+/0}_{GaII}$. The simulation has two free parameters for each defect signature: one pair of Σ^{o}_{n} and $N^{ss}_{tr,eff}$ for $Fe^{0/-}_{GaI}$, $Fe^{0/-}_{GaII}$ and $Ti^{+/0}_{GaII}$, respectively. Increasing Σ^{o}_{n} will lead to a narrowing of the simulated defect signature and shift it to lower

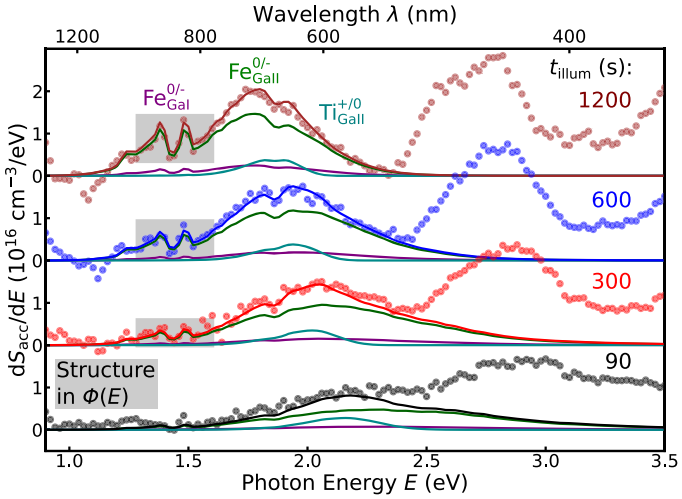

Figure 5. Accumulative SSPC spectra recorded on a EFG-grown β-Ga_2O_3 crystal using different t_{illum}. The spectra were modeled with equation (6), and the models are shown in solid lines. The model parameters are shown in table 2. A feature related to the spectral shape of Φ is marked in gray (see figure 1).

photon energies (see appendix A). Changing $N^{ss}_{tr,eff}$ will scale the simulated defect signature (see appendix A). The parameters which give the model curve shown in figure 4(a) are shown in table 2. The model parameters yield an excellent fit to the recorded data even when modeling different t_{illum} simultaneously, corroborating the validity of employing equation (6). Notably, it was not possible to model T_2^{EFG} using the absorption cross-sections calculated for $Fe^{0/-}_{GaI}$, $Fe^{0/-}_{GaII}$ and $Ti^{+/0}_{GaII}$ (not shown). Thus, we tentatively assign T_1^{EFG} to $Fe^{0/-}_{GaI}$, $Fe^{0/-}_{GaII}$ and $Ti^{+/0}_{GaII}$. However, it is possible that other defects contribute to T_1^{EFG} to a minor extent, i.e., from DLTS measurements, it cannot be ruled out that defects with a concentration below 1×10^{15} cm^{-3} are present in addition to Fe_{GaI}, Fe_{GaII} and Ti_{GaII} that might contribute to T_1^{EFG}.

The simulation takes the spectral shape of the optical excitation represented by Φ (*E*) explicitly into account. In the recorded as well as simulated spectra shown in figure 5, an artifact can be seen at around 1.5 eV which is related to a structure in Φ (*E*) (see figure 1). The corresponding structure can be identified as an artifact in the data as well as the simulation because it does not shift to lower photon energies with increasing t_{illum} as can be expected from features related to optical absorption associated with traps. The fact that modeling based on the measured Φ (*E*) accurately reproduces the artifact as seen in the data further corroborates the validity of the model described in equation (6).

Table 2 shows the comparison of values determined for $N^{ss}_{tr,eff}$ and N_{tr} of Fe_{GaI}, Fe_{GaII} and Ti_{GaII} from SSPC and DLTS measurements, respectively. Notably, all values obtained for $N^{ss}_{tr,eff}$ are lower than the values determined for N_{tr} by a factor of 2–5. Applying a probing volume correction to $N^{ss}_{tr,eff}$ (see equation (3)) will bring the values determined from SSPC measurements closer to the ones obtained from DLTS measurements. Interestingly, a larger deviation between $N^{ss}_{tr,eff}$ and N_{tr} is seen for Ti_{GaII}, as expected for defects more likely to capture electrons. Indeed, Ti_{GaII} is a donor, and hence more prone to capture electrons compared to the acceptor defects Fe_{GaI} and Fe_{GaII} [34, 37]. In accordance, using DLTS, comparatively large apparent cross-sections for electron capture are determined for $Ti^{+/0}_{GaII}$ in contrast to $Fe^{0/-}_{GaI}$ and $Fe^{0/-}_{GaII}$ [8, 9, 23].

5. Summary and conclusion

In summary, we presented a new method to combine SSPC measurements with first-principles calculations which can be used to reveal the identity of optical charge-state transition levels related to defects in wide band gap semiconductors. A method to simulate SSPC spectra using defect-related optical absorption spectra obtained from first-principles calculations based on hybrid-functionals was proposed. The simulations take the experimental conditions for the accumulative SSPC measurements explicitly into account. The thermodynamic charge-state transition levels of $Fe^{0/-}_{GaI}$, $Fe^{0/-}_{GaII}$ and $Ti^{+/0}_{GaII}$ in β-Ga_2O_3 were recently identified [8, 9, 23], and thus served as a test case for the method we developed. Accumulative SSPC measurements were performed on EFG-grown β-Ga_2O_3 crystals and several defect signatures labeled T_1^{EFG}–T_6^{EFG} with onsets for optical absorption between 1.5 eV and 4.3 eV were unveiled. Indeed, we demonstrated how the simulation of accumulatively-recorded derivative SSPC spectra can be used to

Table A1. Overview over standard parameters used for the simulation of SSPC spectra presented here.

Σ_n^o (m^2)	Φ (m^{-2} s^{-1})	t_{illum} (s)	ΔE (meV)	$N_{tr,eff}^{ss}$ (cm^{-3})
2×10^{-20}	10^{18}	10/300	20	10^{16}

identify the optical charge-state transition levels related to $Fe_{GaI}^{0/-}$, $Fe_{GaII}^{0/-}$ and $Ti_{GaII}^{+/0}$ in β-Ga_2O_3. Thus, we were able to assign the signature labeled T_1^{EFG} to $Fe_{GaI}^{0/-}$, $Fe_{GaII}^{0/-}$ as well as $Ti_{GaII}^{+/0}$. Future applications of this approach, as well as its extension to account for optically-induced hole emission processes, may help elucidate the origins of other deep level signatures in β-Ga_2O_3 and other wide-band-gap semiconductors.

Acknowledgments

Financial support is acknowledged from the Research Council of Norway through the FUNDAMENT project (project number: 251131), the Norwegian Micro- and Nano-Fabrication Facility (NorFab, project number: 245963) and the Faculty of Mathematics and Natural Sciences at the University of Oslo via the strategic research initiative FOXHOUND. This work was partially performed under the auspices of the U.S. DOE by Lawrence Livermore National Laboratory under contract DE-AC52-07NA27344, and supported by the Critical Materials Institute, an Energy Innovation Hub funded by the U.S. DOE, Office of Energy Efficiency and Renewable Energy, Advanced Manufacturing Office. We wish to thank Audrius Alkauskas for fruitful collaboration and discussion. We further thank Robert Karsthof, Ole Myren Røhne and Ole Dorholt for wire-bonding of our samples.

Appendix A. Simulation of deep-level transient and steady-state photo-capacitance spectra

A.1. Simulation of deep-level transient spectra

In deep-level transient spectroscopy (DLTS) [1, 7], a rectifying junction is kept a reverse-bias voltage ($V_{rev} < 0$ V) and subjected to a voltage pulse ($V_{pulse} > 0$ V) at a time t_0 which lasts for a duration t_{pulse}. In the following, it is assumed that DLTS measurements are performed on a Schottky junction comprising an n-type semiconductor. Moreover, we assume that a trap exhibiting a concentration of N_{tr} and a single thermodynamic charge-state transition level (E_t) is present in the semiconductor. Prior to applying the voltage pulse, the trap will be empty of electrons in-between the surface of the semiconductor and a depth x_1. x_1 is the depth where the Fermi level (E_F) crosses E_t, and its value will depend on V_{rev}. During the voltage pulse, an additional amount of traps will be filled with electrons, i.e., traps in-between x_1 and a depth x_2 will also be filled with electrons. x_2 is the depth where E_F crosses E_t when the applied bias voltage is equal to $V_{rev} + V_{pulse}$. After the end of the voltage pulse at $t_0 + t_{pulse}$, the charge-state transition level of traps in-between x_2 and x_1 will be above E_F, and thus electron emission will occur until all traps in-between x_2 and x_1 are void of electrons.

The corresponding electron emission is a thermally-activated process, and its rate e_n^{th} can be expressed by [1, 7]:

$$e_n^{th} = \beta \sigma_{na} T^2 \exp\left(-\frac{E_A}{k_B T}\right). \tag{A.1}$$

Here, T is the sample temperature, E_A is the activation energy for thermally-induced electron emission from the trap, σ_{na} is the apparent capture cross section, k_B is Boltzmann's constant and β is a material-specific constant. E_A is the sum of E_t and the corresponding energetic barrier for electron capture (E_b) [1, 21]. Assuming parabolic bands, β can be computed by [1]:

$$\beta = 2\sqrt{3}\left(\frac{2\pi}{h^2}\right)^{\frac{3}{2}} k_B^2 m_{n,eff}. \tag{A.2}$$

Here, h is Planck's constant and $m_{n,eff}$ is the effective mass of electrons in the conduction band. For β-Ga_2O_3, a value of 0.28 m_e was used for $m_{n,eff}$ [53, 54], whereby m_e is the electron mass.

In DLTS, the thermally-induced electron emission is probed by recording the capacitance of the rectifying junction. Particularly, the capacitance transient ($C(t)$) is recorded after the end of the voltage pulse, and is described by [1]

$$C(t) = C_0\left[1 - \frac{N_{tr,probe}}{2N_D} \exp\left(-e_n^{th} t\right)\right], \tag{A.3}$$

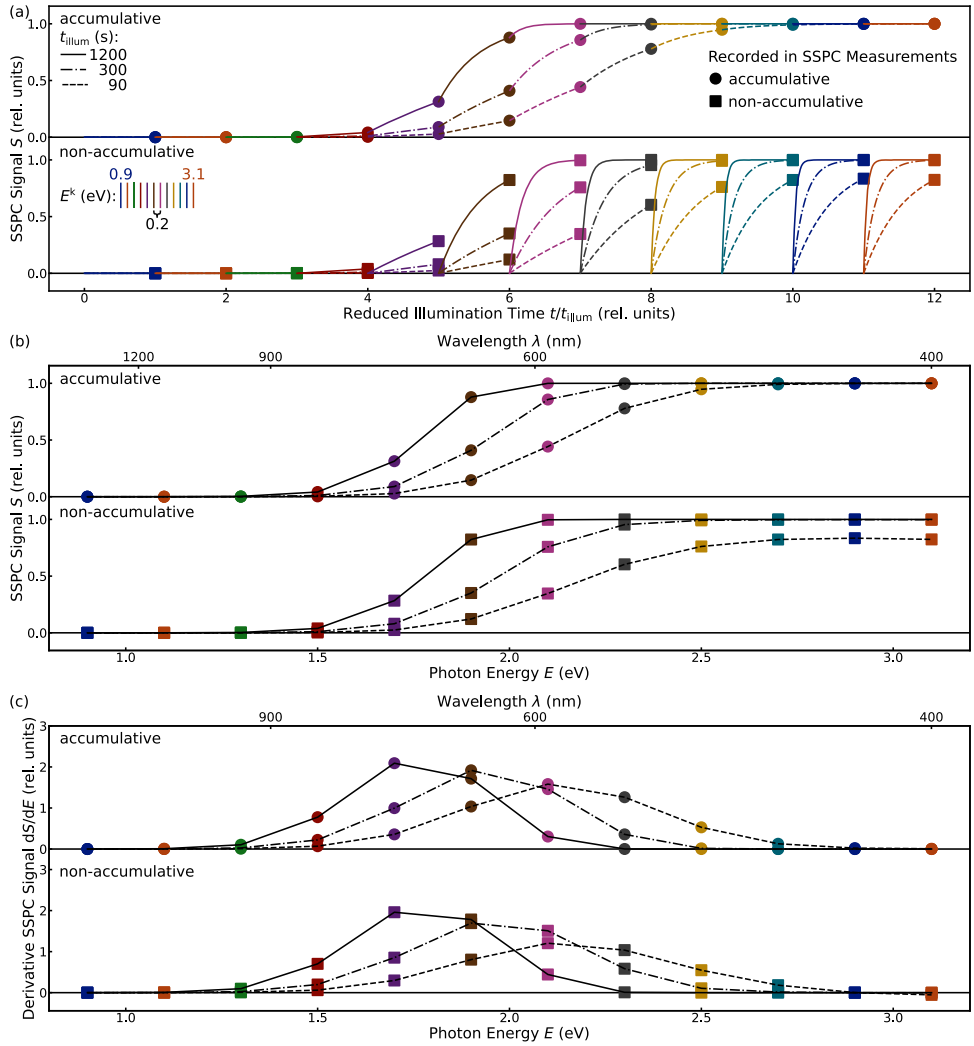

Figure A1. Graphical representation of equations (A.19) and (A.20). Results are shown in dependence of (a) t and (b), (c) E^k. In (b) conventional SSPC spectra are shown, while in (c) derivative SSPC spectra are displayed. Here, the $\sigma^{o}_{n,norm}$ calculated for $Ti^{+/0}_{GaII}$ was used. The simulations were performed using different t_{illum} of 1200 s, 300 s and 30 s. Moreover, the following parameters were used: $\Delta E = 0.2$ eV, $\Sigma^{o}_{n} = 2 \times 10^{-20}$ m^2, $\Phi = 1 \times 10^{18}$ m^{-2} s and $N^{ss}_{tr,eff} = 1 \times 10^{16}$ cm^{-3}.

assuming $N_{tr} \ll N_D$ to be valid. Here, C_0 is the capacitance of the rectifying junction measured prior to the voltage pulse, i.e., the capacitance of the rectifying junction when V_{rev} is applied. N_D is the donor concentration and $N_{tr,probe}$ is the effective trap concentration in the probing volume, i.e., the effective concentration of traps in-between x_2 and x_1. Following the approach outlined by Lang, the DLTS spectra $S_j(T)$ can be constructed, and $S_j(T)$ is defined as [1, 7, 31]:

$$S_j(T) = \frac{1}{t_j} \int_{t_{delay}}^{t_{delay}+t_j} C(t)\, w(t)\, \mathrm{d}t. \tag{A.4}$$

Here, t_{delay} is the time at which the recording of $C(t)$ starts after the end of the voltage pulse, whereas t_j is the duration for which $C(t)$ is recorded/analyzed. $w(t)$ is the weighting function, e.g., a lock-in function [1] or a GS4 filter function [31]. To analyze DLTS measurements, one needs to use more than one specific t_j. Often, $C(t)$ is recorded for a duration $t_{transient}$, and different parts of the transient, represented by t_j, are analyzed in order to obtain different $S_j(T)$. Different $S_j(T)$ essentially correspond to analyzing the recorded $C(t)$ for different values of e^{th}_n (see figure 3 in the manuscript). The recorded $S_j(T)$ can be compared to simulations when combining equation (A.4) with equations (A.1) and (A.3). The free parameters of the simulation are the quantities $N_{tr,probe}$, E_A and σ_{na} which describe the concentration and properties of the trap. Often, one represents DLTS spectra as $2N_D\Delta C/C_0$, whereby $\Delta C = C_0 - C(t = 0\,\mathrm{s})$ can be calculated from $S_j(T)$ as outlined in [1, 55].

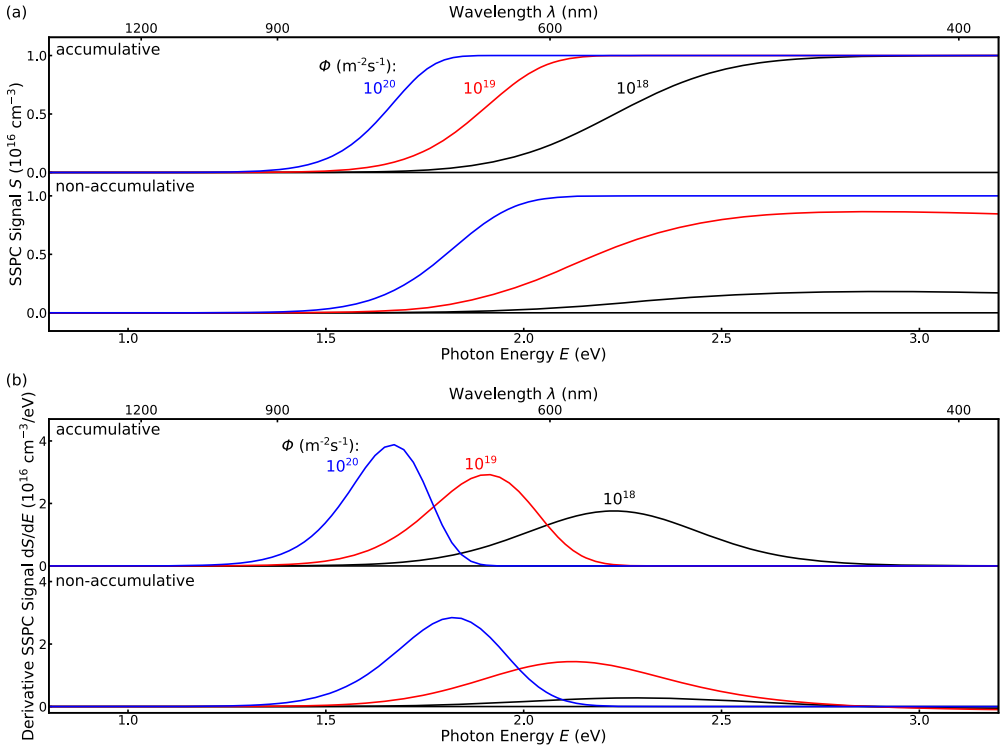

Figure A2. Graphical representation of equations (A.14) and (A.18) for different photon fluxes Φ. Results are shown for (a) conventional and (b) derivative SSPC spectra. Here, the $\sigma^{o}_{n,norm}$ calculated for $Ti^{+/0}_{GaII}$ was used. Moreover, the following parameters were used: $\Delta E = 20$ meV, $\Sigma^{o}_{n} = 2 \times 10^{-20}$ m^2, $t_{illum} = 10$ s and $N^{ss}_{tr,eff} = 1 \times 10^{16}$ cm^{-3}.

As mentioned above, $N_{tr,probe}$ represents the effective trap concentration in-between x_2 and x_1. The actual trap concentration N_{tr} can be determined by using [1]:

$$N_{tr} = \frac{W^2}{x_1^2 - x_2^2} N_{tr,probe}. \tag{A.5}$$

Here, W is the width of the space-charge region when applying V_{rev}. The correction performed in equation (A.5) is often referred to as λ-correction [1, 32].

A.2. Simulation of steady-state photo-capacitance spectra from first-principles calculations

Steady-state photo-capacitance (SSPC) measurements are performed by measuring the photo-capacitance of a rectifying junction after illumination at the photon energy E^k for a duration t_{illum}. In the following, it is assumed that SSPC measurements are performed on a Schottky junction comprising an n-type semiconductor. Moreover, we assume that a trap exhibiting a concentration of N_{tr} and a single thermodynamic charge-state transition level (E_t) is present in the semiconductor.

SSPC spectra ($S\left(E^k, t_{illum}\right)$) are constructed by recording the photo-capacitance ($C_{illum}\left(E^k, t_{illum}\right)$) of the junction at subsequent E^k. $S\left(E^k, t_{illum}\right)$ is usually expressed as [1, 10]:

$$S\left(E^k, t_{illum}\right) = 2\frac{C_{illum}\left(E^k, t_{illum}\right) - C_{dark}}{C_{dark}} N_D = 2\frac{\Delta C_{illum}\left(E^k, t_{illum}\right)}{C_{dark}} N_D = N^{*}_{tr,eff}\left(E^k, t_{illum}\right). \tag{A.6}$$

Here, $\Delta C_{illum}\left(E^k, t_{illum}\right)$ denotes the change in (photo-)capacitance during illumination for t_{illum} at E^k, and C_{dark} represents the capacitance of the junction measured in the dark. $N^{*}_{tr,eff}\left(E^k, t_{illum}\right)$ is the change in the concentration of ionized traps inside the probing volume due to illumination. Notably, the probing volume will usually not be equal to the volume of the space-charge region [1, 28]. Moreover, equation (A.6) assumes $N_D \ll N_{tr}$ to be valid.

$N^{*}_{tr,eff} = S\left(E^k, t_{illum}\right)$ is described by the following differential equation [10]:

$$\frac{dN^{*}_{tr,eff}}{dt} = \sigma^{o}_{n} \Phi N_{tr,eff}, \tag{A.7}$$

when assuming that the photo-ionization process only involves the defect and the conduction band (optically-induced electron emission), i.e., optically-induced hole emission (photo-ionization processes

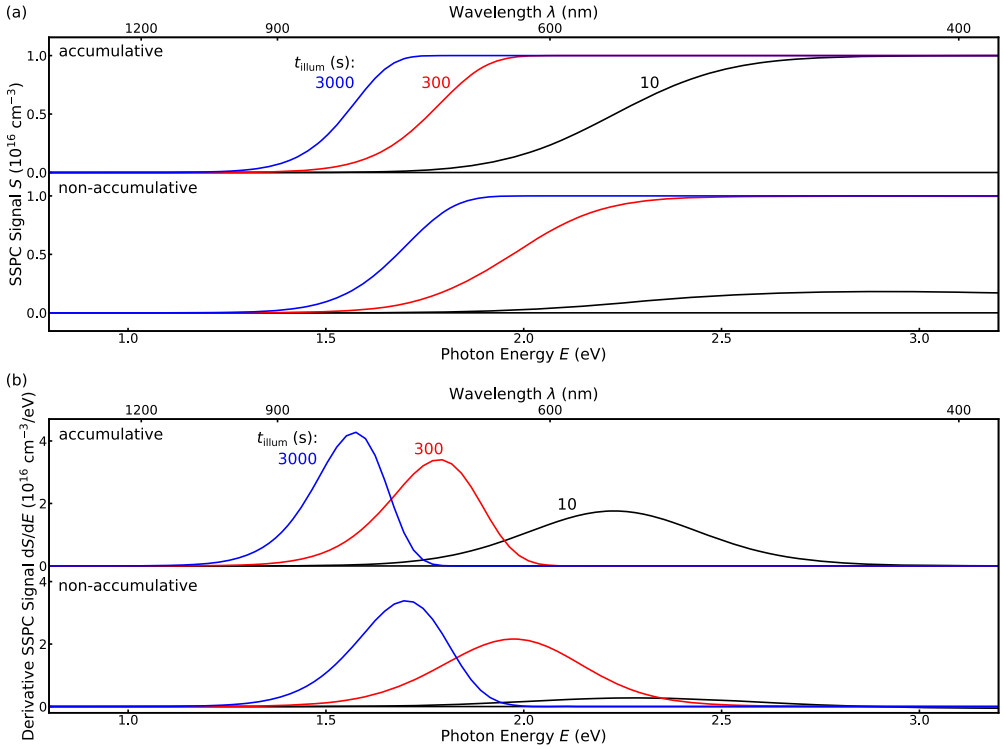

Figure A3. Graphical representation of equations (A.14) and (A.18) for various t_{illum}. Results are shown for (a) conventional and (b) derivative SSPC spectra. Here, the $\sigma^{o}_{n,norm}$ calculated for $Ti^{+/0}_{GaII}$ was used. Moreover, the following parameters were used: $\Delta E = 20$ meV, $\Sigma^{o}_{n} = 2 \times 10^{-20}$ m^2, $\Phi = 1 \times 10^{18}$ m^{-2} s and $N^{ss}_{tr,eff} = 1 \times 10^{16}$ cm^{-3}.

involving the defect and the valence band) can be neglected. Optically-induced hole emission can be neglected if (i) holes are not sufficiently mobile to leave the space-charge region, or (ii) optically-induced hole emission does not occur in the spectral region of interest [10, 28]. In equation (A.7), σ^{o}_{n} represents the absorption cross-section related to the optically-induced electron emission from the defect, whereas Φ denotes the spectral photon flux used for illumination. σ^{o}_{n} and Φ will be functions of E^k. $N_{tr,eff}$ is the concentration of defects inside the probing volume which are not ionized, and hence $N_{tr,eff}$ is equal to $N^{ss}_{tr,eff} - N^{*}_{tr,eff}$. $N^{ss}_{tr,eff}$ is the effective concentration of the defect inside the probing volume. Using this, equation (A.7) becomes:

$$\frac{dN^{*}_{tr,eff}}{dt} = \sigma^{o}_{n}\Phi N^{ss}_{tr,eff} - \sigma^{o}_{n}\Phi N^{*}_{tr,eff}. \tag{A.8}$$

Equation (A.8) describes a first-order, non-homogeneous differential equation. The associated homogeneous differential equation is:

$$\frac{dN^{*}_{tr,eff}}{dt} = -\sigma^{o}_{n}\Phi N^{*}_{tr,eff}. \tag{A.9}$$

This differential equation is solved by:

$$N^{*}_{tr,eff} = A\ \exp\left(-\sigma^{o}_{n}\Phi t\right). \tag{A.10}$$

Here, A is a constant which needs to be chosen according to the boundary condition. A particular solution for equation (A.8) is

$$N^{*}_{tr,eff} = N^{ss}_{tr,eff}. \tag{A.11}$$

The overall solution to equation (A.8) is obtained by adding equations (A.10) and (A.11) together, and hence:

$$N^{*}_{tr,eff} = N^{ss}_{tr,eff} + A\ \exp\left(-\sigma^{o}_{n}\Phi t\right). \tag{A.12}$$

As mentioned above, A needs to be determined from the boundary condition which will depend on the way SSPC measurements are performed. In non-accumulative SSPC measurements, the defect is re-filled with electrons prior to illumination at E^k, and hence the concentration of (photo-)ionized defects prior to illumination at E^k inside the probing volume $\left(N^{*}_{tr,eff}\left(E^k, t = 0\,\mathrm{s}\right)\right)$ will be expressed by:

$$N^{*}_{tr,eff}\left(E^k, t = 0\,\mathrm{s}\right) = 0. \tag{A.13}$$

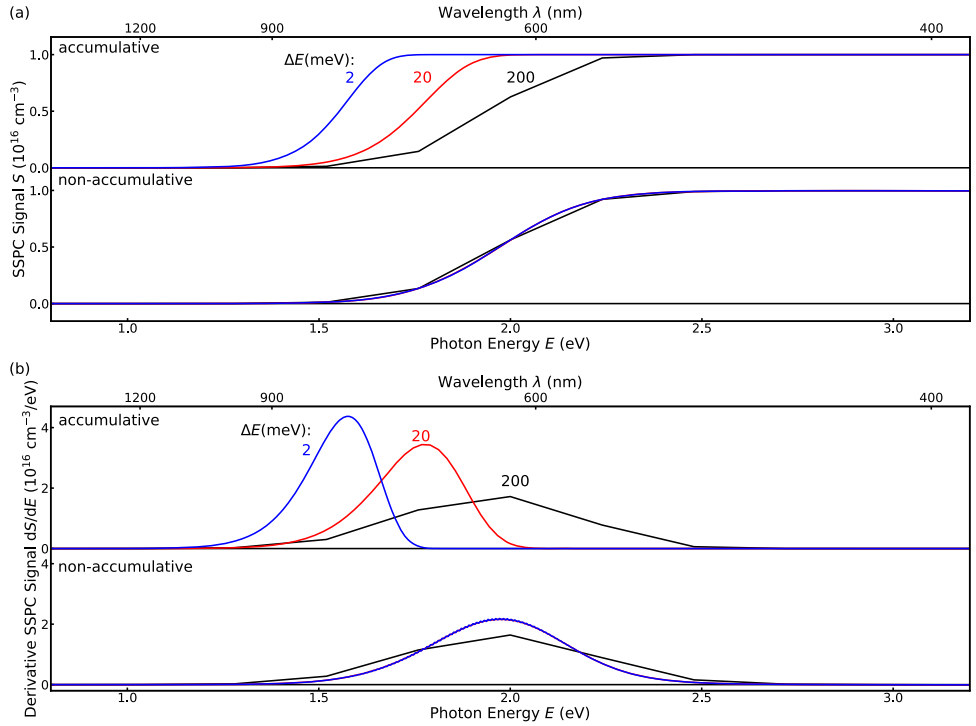

Figure A4. Graphical representation of equations (A.14) and (A.18) for various ΔE. Results are shown for (a) conventional and (b) derivative SSPC spectra. Here, the $\sigma^{o}_{n,norm}$ calculated for $Ti^{+/0}_{GaII}$ was used. Moreover, the following parameters were used: $t_{illum} = 300$ s, $\Sigma^{o}_{n} = 2 \times 10^{-20}$ m^2, $\Phi = 1 \times 10^{18}$ m^{-2} s and $N^{ss}_{tr,eff} = 1 \times 10^{16}$ cm^{-3}.

Thus, A will be equal to $-N_{tr,eff}$, and hence:

$$\begin{aligned} S_{non-acc}\left(E^k, t_{illum}\right) &= N^{ss}_{tr,eff} - N^{ss}_{tr,eff} \exp\left(-\sigma^{o}_{n}\Phi t\right) \\ &= N^{ss}_{tr,eff}\left[1 - \exp\left(-\sigma^{o}_{n}\Phi t_{illum}\right)\right]. \end{aligned} \tag{A.14}$$

Notably, for t_{illum} approaching $\infty\, s$, $S_{non-acc}\left(E^k, t_{illum}\right)$ approaches $N^{ss}_{tr,eff}$. $t_{illum} \rightarrow \infty s$ is equivalent to reaching steady-state conditions, and hence the superscript ss was used for denoting $N^{ss}_{tr,eff}$.

In accumulative SSPC measurements, the rectifying junction under illumination is kept at a fixed reverse-bias voltage while illuminating the junction at different E^k. Importantly, measurements are performed in ascending order of E^k, i.e., $E^k < E^{k+1}$ is valid. For the first measurement performed at E^0, the boundary condition stated in equation (A.13) holds, and thus

$$S_{acc}\left(E^0, t_{illum}\right) = N^{ss}_{tr,eff}\left[1 - \exp\left(-\sigma^{o}_{n}\Phi t_{illum}\right)\right]. \tag{A.15}$$

For illumination at subsequent E^k, the following boundary condition holds:

$$\begin{aligned} N^{*}_{tr,eff}\left(E^k, t = 0\,\mathrm{s}\right) &= N^{*}_{tr,eff}\left(E^{k-1}, t_{illum}\right) \\ &= S_{acc}\left(E^{k-1}, t_{illum}\right) \end{aligned} \tag{A.16}$$

reflecting that when illumination starts, a certain concentration of defects is already photo-ionized due to illumination at E^{k-1}. Thus A is equal to $S_{acc}\left(E^{k-1}, t_{illum}\right) - N^{ss}_{tr,eff}$, and hence:

$$S_{acc}\left(E^k, t_{illum}\right) = N^{ss}_{tr,eff} + \left[S_{acc}\left(E^{k-1}, t_{illum}\right) - N^{ss}_{tr,eff}\right] \exp\left(-\sigma^{o}_{n}\Phi t_{illum}\right) \tag{A.17}$$

is valid for $E^k \neq E^0$. Adding $0 = S_{acc}\left(E^{k-1}, t_{illum}\right) - S_{acc}\left(E^{k-1}, t_{illum}\right)$ on the right hand side, equation (A.17) can be re-written as:

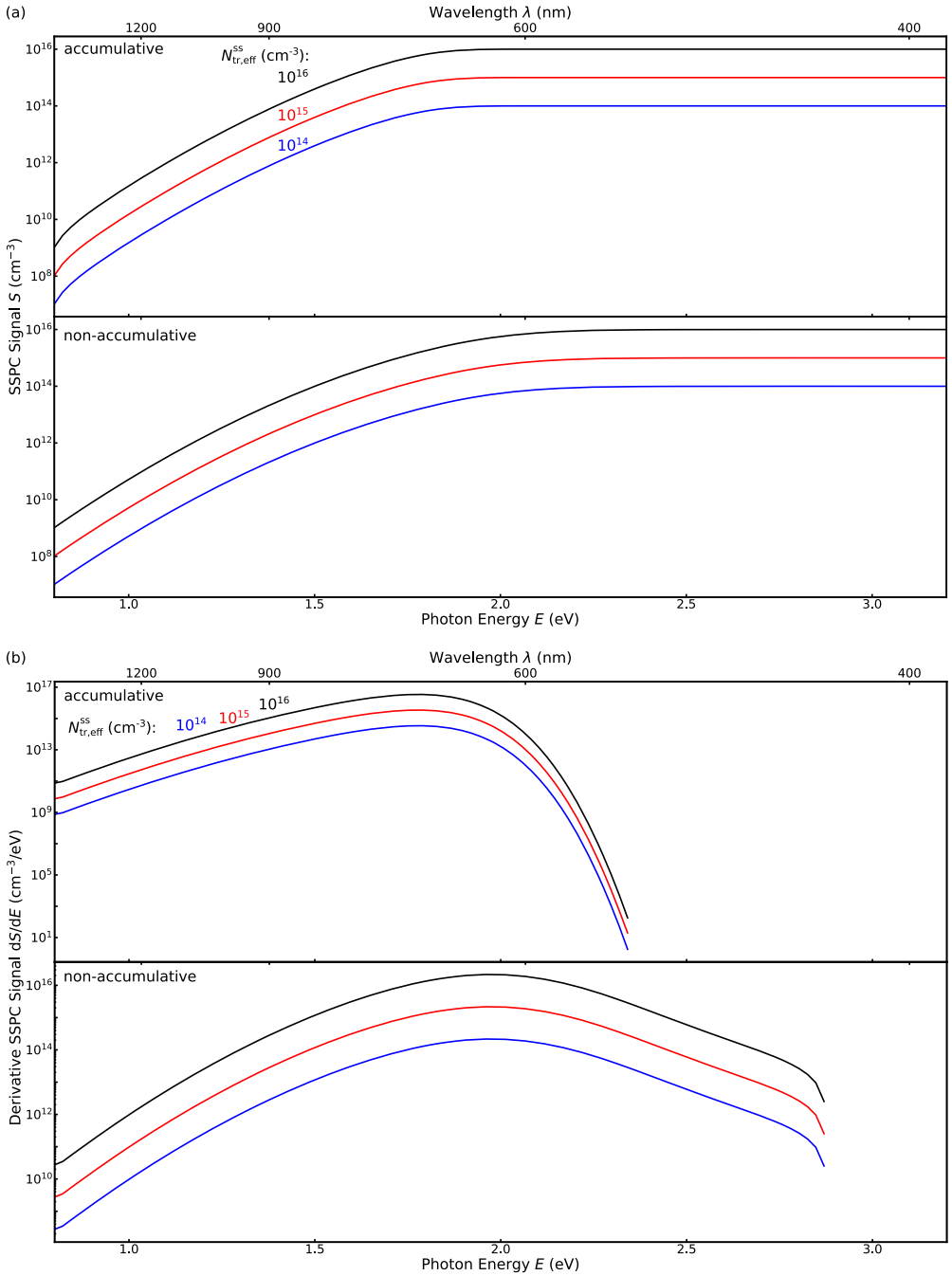

Figure A5. Graphical representation of equations (A.14) and (A.18) for various $N^{ss}_{tr,eff}$. Results are shown for (a) conventional and (b) derivative SSPC spectra. Here, the $\sigma^{o}_{n,norm}$ calculated for $Ti^{+/0}_{GaII}$ was used. Moreover, the following parameters were used: $t_{illum} = 300$ s, $\Sigma^{o}_{n} = 2 \times 10^{-20}$ m^2, $\Phi = 1 \times 10^{18}$ m^{-2} s and $\Delta E = 20$ meV.

$$S_{acc}\left(E^k, t_{illum}\right) = S_{acc}\left(E^{k-1}, t_{illum}\right) - S_{acc}\left(E^{k-1}, t_{illum}\right) + N^{ss}_{tr,eff} + \left[S_{acc}\left(E^{k-1}, t_{illum}\right) - N^{ss}_{tr,eff}\right] \exp\left(-\sigma^{o}_{n}\Phi t_{illum}\right)$$
$$= S_{acc}\left(E^{k-1}, t_{illum}\right) + \left[N^{ss}_{tr,eff} - S_{acc}\left(E^{k-1}, t_{illum}\right)\right]\left[1 - \exp\left(-\sigma^{o}_{n}\Phi t_{illum}\right)\right]. \quad (A.18)$$

This equation is valid for all E^k if $S_{acc}\left(E^0, t_{illum}\right)$ is set to 0.

Equations (A.14) and (A.18) can be expressed more general in the form $S_{acc}\left(E^k, t_{illum}, t\right)$ and $S_{non-acc}\left(E^k, t_{illum}, t\right)$. $S_{acc}\left(E^k, t_{illum}, t\right)$ and $S_{non-acc}\left(E^k, t_{illum}, t\right)$ describe the recorded SSPC spectrum after illumination for a time t at E^k while the junction was illuminated for a duration t_{illum} at all photon energies E^j for which $j < k$ is valid. $S_{acc}\left(E^k, t_{illum}, t\right)$ can be expressed as:

$$S_{acc}\left(E^k, t_{illum}, t\right) = S\left(E^{k-1}, t_{illum}, t_{illum}\right) + \left[N^{ss}_{tr,eff} - S\left(E^{k-1}, t_{illum}, t_{illum}\right)\right]\left[1 - \exp\left(-\sigma^{o}_{n}\Phi t\right)\right], \quad (A.19)$$

while $S_{\mathrm{non-acc}}\left(E^k, t_{\mathrm{illum}}, t\right)$ can be calculated by:

$$S_{\mathrm{non-acc}}\left(E^k, t_{\mathrm{illum}}, t\right) = N_{\mathrm{tr,eff}}^{\mathrm{ss}}\left[1 - \exp\left(-\sigma_{\mathrm{n}}^{\mathrm{o}}\Phi t\right)\right]. \tag{A.20}$$

$\sigma_{\mathrm{n}}^{\mathrm{o}}$ is defined by:

$$\sigma_{\mathrm{n}}^{\mathrm{o}} = \Sigma_{\mathrm{n}}^{\mathrm{o}}\sigma_{\mathrm{n,norm}}^{\mathrm{o}}. \tag{A.21}$$

Here, $\sigma_{\mathrm{n,norm}}^{\mathrm{o}}$ can be obtained from first-principles calculations for a specific trap, while $\Sigma_{\mathrm{n}}^{\mathrm{o}}$ is a free parameter of the simulation.

In the following, graphical representations of equations (A.14), (A.18–A.20) will be shown. Hereby, the calculated $\sigma_{\mathrm{n,norm}}^{\mathrm{o}}$ of $\mathrm{Ti}_{\mathrm{GaII}}^{+/0}$ was used. In table A1, the standard values for the simulation parameters are stated. Φ is assumed to be constant for all photon energies, and ΔE is the energy step between two subsequent E^k, i.e., $\Delta E = E^{k+1} - E^k$ is valid.

Figure A1 displays graphical representations of equations (A.19) and (A.20). Figure A1(a) shows the dependence on t, while figures A1(b) and (c) show the corresponding dependence on E^k. Notably, for the same experimental conditions, non-accumulative SSPC measurements will reach steady-state conditions for longer t_{illum} compared to accumulative SSPC measurements. Generally, longer t_{illum} are associated with steps in SSPC spectra shifting to lower photon energies and becoming steeper.

In figures A2–A5, the influence of a particular parameter on equations (A.14) and (A.18) is shown. For longer t_{illum} and higher Φ, steps in S_{acc} as well as $S_{\mathrm{non-acc}}$ will shift to lower photon energies and become steeper. The corresponding changes are more notable for accumulative SSPC spectra under the same experimental conditions. Only S_{acc} exhibits a change depending on ΔE. For S_{acc} as well as $S_{\mathrm{non-acc}}$, $N_{\mathrm{tr,eff}}^{\mathrm{ss}}$ is a scaling factor.

ORCID iDs

C Zimmermann https://orcid.org/0000-0003-3708-6074
Y Kalmann Frodason https://orcid.org/0000-0001-9151-2084
J B Varley https://orcid.org/0000-0002-5384-5248
L Vines https://orcid.org/0000-0001-5759-7192

References

[1] Blood P and Orton J W 1992 *The Electrical Characterization of Semiconductors: Majority Carriers and Electron States* (Techniques of Physics) (New York: Academic)
[2] Van de Walle C G and Neugebauer J 2004 First-principles calculations for defects and impurities: applications to III-nitrides *J. Appl. Phys.* **95** 3851–79
[3] Pearton S J, Yang J, Cary P HIV, Ren F, Kim J, Tadjer M J and Mastro M A 2018 A review of Ga_2O_3 materials, processing, and devices *Appl. Phys. Rev.* **5** 011301
[4] Higashiwaki M, Sasaki K, Murakami H, Kumagai Y, Koukitu A, Kuramata A, Masui T and Yamakoshi S 2016 Recent progress in Ga_2O_3 power devices *Semicond. Sci. Technol.* **31** 034001
[5] Nakagomi S, Momo T, Takahashi S and Kokubun Y 2013 Deep ultraviolet photodiodes based on β-Ga_2O_3/SiC heterojunction *Appl. Phys. Lett.* **103** 072105
[6] Nakagomi S, Sato T, Takahashi Y and Kokubun Y 2015 Deep ultraviolet photodiodes based on the β-Ga_2O_3/GaN heterojunction *Sensors Actuators* A **232** 208–13
[7] Lang D V 1974 Deep-level transient spectroscopy: a new method to characterize traps in semiconductors *J. Appl. Phys.* **45** 3023–32
[8] Eide Ingebrigtsen M, Varley J B, Kuznetsov A Y, Svensson B G, Alfieri G, Mihaila A, Badstübner U and Vines L 2018 Iron and intrinsic deep level states in Ga_2O_3 *Appl. Phys. Lett.* **112** 042104
[9] Ingebrigtsen M E, Kuznetsov A Y, Svensson B G, Alfieri G, Mihaila A, Badstübner U, Perron A, Vines L and Varley J B 2019 Impact of proton irradiation on conductivity and deep level defects in β-Ga_2O_3 *APL Mater.* **7** 022510
[10] Chantre A, Vincent G and Bois D 1981 Deep-level optical spectroscopy in GaAs *Phys. Rev.* B **23** 5335
[11] Farzana E, Ahmadi E, James S S, Arehart A R and Ringel S A 2018 Deep level defects in Ge-doped (010) β-Ga_2O_3 layers grown by plasma-assisted molecular beam epitaxy *J. Appl. Phys.* **123** 161410
[12] Zhang Z, Farzana E, Arehart A R and Ringel S A 2016 Deep level defects throughout the bandgap of (010) β-Ga_2O_3 detected by optically and thermally stimulated defect spectroscopy *Appl. Phys. Lett.* **108** 052105
[13] Farzana E, Chaiken M F, Blue T E, Arehart A R and Ringel S A 2019 Impact of deep level defects induced by high energy neutron radiation in β-Ga_2O_3 *APL Mater.* **7** 022502
[14] Polyakov A Y, Smirnov N B, Shchemerov I V, Yakimov E B, Yang J, Ren F, Yang G, Kim J, Kuramata A and Pearton S J 2018 Point defect induced degradation of electrical properties of Ga_2O_3 by 10 MeV proton damage *Appl. Phys. Lett.* **112** 032107
[15] Polyakov A Y *et al* 2018 Defects responsible for charge carrier removal and correlation with deep level introduction in irradiated β-Ga_2O_3 *Appl. Phys. Lett.* **113** 092102
[16] Polyakov A Y, Smirnov N B, Shchemerov I V, Gogova D, Tarelkin S A and Pearton S J 2018 Compensation and persistent photocapacitance in homoepitaxial Sn-doped β-Ga_2O_3 *J. Appl. Phys.* **123** 115702

[17] Polyakov A Y, Smirnov N B, Shchemerov I V, Pearton S J, Fan R, Chernykh A V and Kochkova A I 2018 Electrical properties of bulk semi-insulating β-Ga_2O_3 (Fe) *Appl. Phys. Lett.* **113** 142102

[18] Nakano Y 2017 Electrical characterization of β-ga_2O_3 single crystal substrates *ECS J. Solid State Sci. Technol.* **6** P615–7

[19] Krukau A V, Vydrov O A, Izmaylov A F and Scuseria G E 2006 Influence of the exchange screening parameter on the performance of screened hybrid functionals *J. Chem. Phys.* **125** 224106

[20] Freysoldt C, Grabowski B, Hickel T, Neugebauer J, Kresse G, Anderson J and Van de Walle C G 2014 First-principles calculations for point defects in solids *Rev. Mod. Phys.* **86** 253

[21] Wickramaratne D, Dreyer C E, Monserrat B, Shen J-X, Lyons J L, Alkauskas A and Van de Walle C G 2018 Defect identification based on first-principles calculations for deep level transient spectroscopy *Appl. Phys. Lett.* **113** 192106

[22] Alkauskas A, McCluskey M D and Van de Walle C G 2016 Tutorial: Defects in semiconductors - combining experiment and theory *J. Appl. Phys.* **119** 181101

[23] Zimmermann C, Frodason Y K, Barnard A W, Varley J B, Irmscher K, Galazka Z, Karjalainen A, Meyer W E, Auret F D and Vines L 2020 Ti- and Fe-related charge transition levels in β-Ga_2O_3 *Appl. Phys. Lett.* **116** 072101

[24] Kopylov A A and Pikhtin A N 1975 Influence of temperature on spectra of optical absorption by deep levels in semiconductors *Sov. Phys. - Solid State* **16** 1200–3

[25] Aida H, Nishiguchi K, Takeda H, Aota N, Sunakawa K and Yaguchi Y 2008 Growth of β-Ga_2O_3 single crystals by the edge-defined, film fed growth method *Jpn. J. Appl. Phys.* **47** 8506–9

[26] Kuramata A, Koshi K, Watanabe S, Yu Y, Masui T and Yamakoshi S 2016 High-quality single crystals grown by edge-defined film-fed growth *Japan. J. Appl. Phys.* **55** 1202A2

[27] Ingebrigtsen M E, Vines L, Alfieri G, Mihaila A, Badstübner U, Svensson B G and Kuznetsov A 2017 Bulk β-Ga_2O_3 with (010) and (201) surface orientation: Schottky contacts and point defects *Mater. Sci. Forum* **897** 755–8

[28] Zimmermann C, Rønning V, Frodason Y K, Varley J B, Bobal V and Vines L 2020 Primary intrinsic defects and their charge transition levels in β-Ga_2O_3 *Phys. Rev. Mater.* (submitted)

[29] Passlack M, Hunt N E J, Schubert E F, Zydzik G J, Hong M, Mannaerts J P, Opila R L and Fischer R J 1994 Dielectric properties of electron beam deposited Ga_2O_3 films *Appl. Phys. Lett.* **64** 2715–7

[30] Svensson B G, Rydén K-H and Lewerentz B M S 1989 Overlapping electron traps in n-type silicon studied by capacitance transient spectroscopy *J. Appl. Phys.* **66** 1699–704

[31] Istratov A A 1997 New correlation procedure for the improvement of resolution of deep level transient spectroscopy of semiconductors *J. Appl. Phys.* **82** 2965–8

[32] Irmscher K, Galazka Z, Pietsch M, Uecker R and Fornari R 2011 Electrical properties of β-Ga_2O_3 single crystals grown by the czochralski method *J. Appl. Phys.* **110** 063720

[33] Ridley B K 1978 Multiphonon, non-radiative transition rate for electrons in semiconductors and insulators *J. Phys. C: Solid State Phys.* **11** 2323–41

[34] Alkauskas A, Yan Q and Van de Walle C G 2014 First-principles theory of nonradiative carrier capture via multiphonon emission *Phys. Rev.* B **90** 075202

[35] Bonch-Bruevich V L 1959 *Fiz. Tverd. Tella* **182**

[36] Gummel H and Lax M 1955 Thermal ionization and capture of electrons trapped in semiconductors *Phys. Rev.* **97** 1469

[37] Pässler R 1976 Relationships between the nonradiative multiphonon carrier-capture properties of deep charged and neutral centres in semiconductors *Phys. Status Solidi* B **78** 625–35

[38] Kresse G and Furthmüller J 1996 Efficient iterative schemes for ab initio total-energy calculations using a plane-wave basis set *Phys. Rev.* B **54** 11169

[39] Freysoldt C, Neugebauer J and Van de Walle C G 2009 Fully ab initio finite-size corrections for charged-defect supercell calculations *Phys. Rev. Lett.* **102** 016402

[40] Kumagai Y and Oba F 2014 Electrostatics-based finite-size corrections for first-principles point defect calculations *Phys. Rev.* B **89** 195205

[41] Gake T, Kumagai Y, Freysoldt C and Oba F 2020 Finite-size corrections for defect-involving vertical transitions in supercell calculations *Phys. Rev.* B **101** 020102

[42] Stoneham A M 1975 *Theory of Defects in Solids* (Oxford: Oxford University Press)

[43] Alkauskas A, Lyons J L, Steiauf D and Van de Walle C G 2012 First-principles calculations of luminescence spectrum line shapes for defects in semiconductors: the example of GaN and ZnO *Phys. Rev. Lett.* **109** 267401

[44] White A M, Dean P J and Porteous P 1976 Photocapacitance effects of deep traps in epitaxial GaAs *J. Appl. Phys.* **47** 3230–9

[45] Varley J B, Janotti A, Franchini C and Van de Walle C G 2012 Role of self-trapping in luminescence and p-type conductivity of wide-band-gap oxides *Phys. Rev.* B **85** 081109

[46] Kananen B E, Giles N C, Halliburton L E, Foundos G K, Chang K B and Stevens K T 2017 Self-trapped holes in β-Ga_2O_3 crystals *J. Appl. Phys.* **122** 215703

[47] Furukawa Y 1967 Trap levels in gallium arsenide *Japan. J. Appl. Phys.* **6** 675

[48] Bhandari S, Zvanut M E and Varley J B 2019 Optical absorption of Fe in doped Ga_2O_3 *J. Appl. Phys.* **126** 165703

[49] Saleh M, Varley J B, Jesenovec J, Bhattacharyya A, Krishnamoorthy S, Swain S and Lynn K 2020 Degenerate doping in β-Ga_2O_3 single crystals through Hf-doping *Semicond. Sci. Technol.* **35** 04LT01

[50] Bhandari S and Zvanut M E 2020 Optical transitions for impurities in Ga_2O_3 as determined by photo-induced electron paramagnetic resonance spectroscopy *J. Appl. Phys.* **127** 065704

[51] Lenyk C A, Gustafson T D, Halliburton L E and Giles N C 2019 Deep donors and acceptors in β-Ga_2O_3 crystals: determination of the $Fe^{2+/3+}$ level by a noncontact method *J. Appl. Phys.* **126** 245701

[52] Polyakov A Y, Lee I-H, Smirnov N B, Shchemerov I V, Vasilev A, Chernykh A V and Pearton S J 2020 Electric field dependence of major electron trap emission in bulk β-Ga_2O_3: Poole-frenkel effect versus phonon-assisted tunneling *J. Phys. D: Appl. Phys.* **53** 304001

[53] Janowitz C *et al* 2011 Experimental electronic structure of In_2O_3 and Ga_2O_3 *New J. Phys.* **13** 085014

[54] Mock A, Korlacki R, Briley C, Darakchieva V, Monemar B, Kumagai Y, Goto K, Higashiwaki M and Schubert M 2017 Band-to-band transitions, selection rules, effective mass, and excitonic contributions in monoclinic β-Ga_2O_3 *Phys. Rev.* B **96** 245205

[55] Åberg D 2001 Capacitance spectroscopy of point defects in silicon and silicon carbide *PhD Thesis* KTH, Royal Institute of Technology Stockholm